The open ocean sensible heat flux and its significance for Arctic boundary layer mixing during early fall

Manisha Ganeshan[1], Dong L. Wu[2]

[1]Goddard Earth Sciences Technology and Research Studies and Investigations, USRA, Greenbelt, 20771, U.S.A.
5   [2]NASA Goddard Space Flight Center, Greenbelt, 20771, U.S.A.

Correspondence to: Manisha Ganeshan (mganeshan@usra.edu)

Abstract. The increasing ice-free area during late summer has transformed the Arctic to a climate system with more dynamic boundary layer clouds and seasonal sea ice growth. The open ocean sensible heat flux, a crucial mechanism of excessive ocean heat loss to the atmosphere during the fall freeze season, is speculated to play an important role in the

10   recently observed cloud cover increase and boundary layer (BL) instability. However, lack of observations and understanding of the resilience of the proposed mechanisms, especially in relation to meteorological and interannual variability, has left a poorly constrained BL parameterization scheme in Arctic climate models. In this study, we use multi-year Japanese cruise ship observations from R/V Mirai over the open Arctic Ocean to characterize the surface sensible heat flux (SSHF) during early fall and investigate its contribution to BL turbulence. It is found that mixing by SSHF is favored

15   during episodes of high surface wind speed, and is also influenced by the prevailing cloud regime. The deepest boundary layers and maximum ocean-atmosphere temperature difference is observed during cold air advection (associated with the stratocumulus regime), yet, contrary to previous speculation, the efficiency of sensible heat exchange is low. On the other hand, the SSHF contributes significantly to BL mixing during the uplift (low-pressure) followed by the highly stable (stratus) regime. Overall, it can explain ~10% of the open ocean BL height variability, whereas cloud (moisture and radiative) driven

20   mechanisms appear to be the other dominant source of convective turbulence. Nevertheless, there is strong interannual variability in the relationship between the SSHF and the BL height which can be intensified by the changing occurrence of Arctic climate patterns, such as positive surface wind speed anomalies and more frequent conditions of uplift. This study highlights the need for comprehensive boundary layer observations like the R/V Mirai for better understanding and predicting the dynamic nature of the Arctic climate.

1

1 Introduction

The recent decline of the Arctic sea ice during late summer (Aug-Sep) has raised several questions for the new climate system, for example, the response of boundary layer clouds and the feedback to sea ice recovery. Turbulent heat fluxes over the ice-free ocean are expected to play an important role under these circumstances. The aim of this study is to provide a better understanding of the role of surface sensible heat flux in the formation of oceanic boundary layer and dissipating ocean heat to the atmosphere during late summer and early fall.

Model simulations of the 21st century climate have suggested that even if the Arctic Ocean were to become completely ice-free in summer, the loss of excess heat to the atmosphere through enhanced ocean (sensible and latent) heat fluxes during October-December months would enable the recovery of sea ice (Tietsche et al. 2011). Ship-based observations during the fall of 2010 have similarly indicated the importance of the ocean sensible heat flux for the onset of the annual freeze cycle (Inoue and Hori 2011). The authors suggested that the cold air outbreak in the wake of cyclogenesis enabled significant cooling of the upper ocean (and freeze onset; Inoue and Hori 2011). Presently, however, there is limited observational guidance for the open ocean heat fluxes and the efficiency of turbulent heat exchange during such events.

The rapid sea-ice retreat in recent years has also raised speculation that the increased air-sea temperature gradients may contribute to reduced boundary layer stability and associated cloud changes (Kay and Gettelman 2009; Schweiger et al. 2008). For example, observations from satellites (Kay and Gettelman 2009; Wu and Lee 2012) and ground stations (Eastman and Warren 2010) suggest a general increase in the low cloud cover over the ice-free Arctic Ocean during fall, especially in regions of reduced atmospheric stability (Kay and Gettelman 2009). Studies have also shown an increase in the mid-level cloud cover (and simultaneous decrease in low clouds) indicating a deepening of the Arctic boundary layer (Sato et al. 2012; Schweiger et al. 2008; Palm et al. 2010). This has also been attributed mainly to the enhanced air-sea temperature difference and resulting upward sensible heat flux (Sato et al. 2012; Schweiger et al. 2008). Despite the observed cloud changes, no direct measurements have been made to quantify the open ocean surface fluxes or its influence on boundary layer mixing. As this area continues to increase in a warmer climate, it becomes more important to fully understand and characterize the changes in cloud cover and the underlying boundary layer processes.

Observations over sea ice show that mixing in the Arctic boundary layer is primarily driven by clouds and cloud-top radiative cooling (Tjernstrom et al. 2004; Inoue et al. 2005; Morrison et al. 2011; Shupe et al. 2013), which can be more significant than surface turbulent fluxes (Curry et al. 2000; Morrison et al. 2012; Shupe et al. 2013; Nicholls and Leighton 1986). Such a BL represents the situation arising from strongly insulating sea ice that prevents efficient turbulent heat exchange at the surface. Over the open ocean, the air-sea interaction can be more pronounced. For example, it has been suggested that surface heat and moisture fluxes lead to boundary layer "roll" clouds during cold air outbreak events over the open Arctic Ocean (Klein et al. 2009). In this study, using multi-year ship-based observations, we investigate the variability of the open ocean sensible heat flux, and more importantly its contribution to boundary layer mixing (and turbulent heat exchange) under varying weather (and cloud) regimes.

2 Datasets

Surface and upper-air meteorological data from the ice-strengthened research vessel (R/V Mirai) operated by the Japan Agency for Marine-Earth Science and Technology are analyzed in this study. The vessel surveyed the ice-free regions mainly in the vicinity of Beaufort and Chukchi seas (from 125° W - 175° E longitude and between 60° - 80° N latitude).

5 Data were collected during September and early October of the years 2002 (Fujiyoshi and Shimada 2002), 2004 (Fujiyoshi and Shimada 2004), 2008 (Kurita and Yoneyama 2008), 2009 (Inoue and Yoneyama 2009), 2010 (Inoue 2010) and 2013 (Inoue 2013). On account of the retreating sea ice, recent observations were collected in more northern latitudes compared to earlier years (Fig. 1; Sato et al. 2012; Inoue and Hori 2011). The year 2013, however, is an exception when observations were primarily collected at a fixed point (72.75 °N and 168.25 °W) as part of the Arctic Research Collaboration for the

10 Radiosonde Observing System (ARCROSE) experiment (Inoue et al. 2015; Kawaguchi et al. 2015). The radiosonde data include profiles of temperature, pressure, winds, and relative humidity, typically sampled at 3 to 12 hour intervals with vertical resolution ranging from 40 m in the lower levels to around 70 m in the mid-troposphere. In order to exclude the near-surface contamination due to warming and cooling of the ship body, a minimum height threshold of 100 m is imposed to ensure quality data of the atmospheric profiles.

15   Also used in the R/V Mirai data analysis are independent, quality controlled observations of surface meteorological variables, viz., 10-minute average values of sea surface temperature (SST), surface air temperature (SAT), surface pressure, and surface horizontal wind speed (V_{surf}). The SAT and V_{surf} are measured at 21 m and 25 m above sea level, respectively. These measurements are used to estimate the surface sensible heat flux (SSHF) at the time of radiosonde launches. A total of 876 contemporaneous samples of boundary layer structure and SSHF (excluding missing data) are analyzed from all cruises.

20 Thus, this dataset provides a unique and valuable survey of Arctic boundary layer properties over the open ocean (Fig. 1), complementing other observational efforts carried out mainly on the central polar ice pack (Tjernstrom et al. 2004; Shupe et al. 2013) and coastal/continental Arctic regions (Eastman and Warren 2010).

3 Methods

3.1 Estimation of surface sensible heat flux

25 The product of the wind speed, and the temperature difference between the sea surface and overlying air (ΔT), is a common estimate of the SSHF (Fairall et al. 1996; Bourassa et al. 2010; Inoue et al. 2011). In this study, the SSHF is calculated using the following equation,

$$SSHF \quad = \quad \rho C_p C_H V_{surf} (\Delta T), \tag{1}$$

30

where $\quad \Delta T = SST - SAT$, °C,

3

V_{surf} = surface horizontal wind speed, m s^{-1}

ρ = air density, kg m^{-3}

C_p = specific heat capacity of air, J kg^{-1} K^{-1}

C_H = transfer coefficient for SSHF (based on winds measured at 20 m height)

5

The values of the constants ρ, C_p, and C_H, are adopted from Inoue et al. (2011). Based on Eq. 1, positive values of SSHF will indicate upward surface sensible heat flux (from the ocean to the atmosphere).

3.2 Determination of boundary layer height

The height of the well-mixed boundary layer is calculated using the parcel-based method, as illustrated in Fig. 2. In this

10   method, a surface parcel is assumed to ascend along a dry adiabat up to the lifting condensation level (LCL), and along a moist adiabat thereafter (denoted by red dashed line in Fig. 2). There is no striking difference in the slopes of the dry and moist adiabats in Fig. 2, as they are nearly parallel in a cold environment. The height of the boundary layer (BL) is computed as the level where the parcel temperature falls below the environment temperature by a value of 0.6 °K or more. For most soundings, this level is coincident with the cloud top or the base of the temperature inversion (as shown in Fig. 2). To

15   comprehend the complex Arctic BL processes, we also examine the influence of BL clouds as described in the following subsection.

The boundary layer over the open Arctic Ocean is found to be mixed or neutral (>90% of the time), in agreement with Sato et al. (2012). The wind speed variance in the BL is typically less than 30% of the mean, suggesting negligible mechanical turbulence for most cases. The Arctic BLs, thus, appear to be primarily mixed by convective fluxes. In a well-

20   mixed BL, the surface turbulent fluxes decrease linearly with height (Holton 2004). Hence, we examine the correlation between the SSHF and the BL height on a profile-by-profile basis. A good correlation implies that the SSHF controls the convective turbulence in the BL. In the case of a poor correlation, factors such as cloud or moisture driven turbulence may influence the BL height (Morrison et al. 2012; Shupe et al. 2013). We investigate the BL cloud statistics as described below. Note that a *bottom-up* approach is used to identify the boundary layer top, which ensures that clouds identified within the BL

25   are always coupled to the *surface*.

3.3 Estimation of boundary layer cloud thickness ratio

Based on past studies over sea ice, the Arctic is found to be mostly cloudy, and the cloud-driven turbulence is known to control the BL height variability (Tjernstrom et al. 2004; Shupe et al. 2013). Low clouds coupled to the boundary layer may generate convective turbulence from above (Curry et al. 2000; Morrison et al. 2012; Shupe et al. 2013), thereby weakening

30   the correlation between the SSHF and BL height. It is therefore important to consider the effect of boundary layer clouds in this study. For this purpose, the BL cloud thickness ratio is calculated as the percentage ratio of cloud layer within the BL. The cloud-base is defined as the first layer above the surface where the relative humidity (RH) equals 90% or more (as in

4

Sato et al. 2012), and the cloud layer is calculated as the vertical integral of all layers within the boundary layer that exceed 90% RH. As an example, for the profile shown in Fig. 2 (inset), the cloud-base and BL heights are calculated as 580 m and 1180 m respectively, and the BL cloud thickness ratio is estimated to be ~50%.

4 Results

4.1 Characteristics of SSHF over the open Arctic Ocean

Figure 3 shows the distribution of the SSHF, the temperature gradient between sea surface and air (ΔT), and the surface wind speeds (V_{surf}), based on multi-year observations. The lack of meaningful differences in the yearly SSHF median values suggests that its interannual variability is not significant at the 95% confidence level. The correlation between SSHF and ΔT (*correlation coefficient* = 0.77) is found to be higher than that of SSHF and V_{surf} (*correlation coefficient* = 0.45). The distribution in Fig. 3 (a) indicates that more positive SSHF values, and a heavier tail (barring outliers), occur in recent years (2009, 2010, 2013). It appears that more negative SAT values (not shown) may contribute to the broader ΔT and SSHF distributions observed during 2009 and 2010 (Figs. 3 (a) and (b)). (In general, the ΔT appears to be more strongly influenced by SAT rather than SST).

As the SSHF can be sensitive to the ΔT variability during fall, it is particularly interesting to explore its relationship with negative SATs. In model simulations, the occurrence of cold air advection (CAA) events and increased ΔT, is known to release copious amounts of ocean heat flux and trigger the seasonal recovery of sea ice (Deser et al. 2010; Kolstad and Bracegirdle 2008). Models also project that future occurrences of CAA may spread further poleward along the retreating sea ice margin (Kolstad and Bracegirdle 2008). In spite of recent observations and modeling efforts (Inoue and Hori 2011; Klein et al. 2009), there are limited measurements of actual surface fluxes during such events. In the following sections, using ship-based measurements, we investigate the instantaneous relationship between the surface sensible heat flux and the boundary layer height, which qualitatively represents the efficiency of turbulent heat exchange between the ocean and the atmosphere.

4.2 The SSHF contribution to boundary layer mixing

Figure 4 (a) shows that a weak positive relationship exists between the SSHF and BL height, which can explain up to 10% of the BL height variability. Contrary to expectations, this relationship is not found to depend on the ocean-atmosphere temperature gradient (ΔT). Instead, the correlation coefficient (r) is sensitive to the surface wind speeds (V_{surf}; Fig. 4 (b)) suggesting that the surface-generated turbulent mixing is favored during episodes of strong winds, and is independent of the ΔTs.

Additionally, low-level clouds, which are known to generate turbulence in the Arctic BL, may influence the correlation. Therefore, we closely inspect the behavior of the correlation coefficient (r) under varying cloud regimes in the following subsection.

5

4.2.1 Effects of cloud regime

In the Arctic, large-scale atmospheric processes are mainly responsible for the occurrence and sustenance of low cloud cover (Herman and Goody 1976; Morrison et al., 2012; Solomon et al., 2014). Barton et al. (2012) recently classified Arctic clouds based on the background dynamic and thermodynamic state of the lower troposphere. They identified four robust meteorological regimes based on the lower tropospheric stability or the potential temperature difference between the surface and 700 mb (θ_{700} - θ_{surf}), and the 500 mb pressure vertical velocity (ω_{500}). The first three regimes have positive ω_{500} values indicating weak subsidence, and differ only in their lower tropospheric stability (θ_{700} - θ_{surf}; Barton et al. 2012). The fourth atmospheric state comprises the uplift regime (characterized by rising motion or negative ω_{500} values), which is only found to occur 10-15% of the time (Barton et al. 2012; Taylor et al. 2015). The subsidence regimes typically have cloud bases within the boundary layer, and are characterized by increasing cloud-top/BL height with decreasing stability (Barton et al. 2012). During the uplift regime, on the other hand, the cloud fraction peaks in the free troposphere above the boundary layer (Barton et al. 2012). In our study, the focus is on the boundary layer height variability therefore we will not be studying clouds with cloud-base above the BL. Moreover, in lieu of the pressure vertical velocity (ω_{500}), we examine the surface pressure to distinguish between the uplift and subsidence regimes.

The bottom panel of Figure 5 (a) shows the frequency distribution of BL cloud thickness ratio during fall. Three distinct BL cloud types emerge, with thickness ratios peaking at 5%, 65%, and 95% (Fig. 5 (a)). Consequently, the observations are divided into three groups consisting of low (<20%), medium (20-80%), and high (>80%) BL cloud thickness ratios, respectively. Note that threshold pairs other than 20-80% (such as 10-90% and 25-75%) were tested for classification purposes, and the results were found to remain robust. Table 1 shows the occurrence frequency, mean surface pressure, and the lower tropospheric stability (θ_{700} - θ_{surf}) associated with each group, while Figs. 5 (b)-(d) show the average temperature and moisture profiles. Significantly lower pressure conditions (99% confidence level) are associated with the low BL cloud thickness group, which occurs roughly 15% of the time. While upper level clouds may be present, a vast majority of the cases do not have boundary layer clouds (Fig. 5 (b)). Therefore this group is synonymous with the uplift regime described by Barton et al. (2012). On the other hand, the top panel of Figure 5 (a) suggests that BL clouds are favored in a subsiding environment (high-pressure conditions), consistent with Barton et al. (2012).

For the group with high BL cloud thickness (greater than 80%), the relatively strong lower tropospheric stability (Table 1) and shallow BL height (Fig. 5 (d)) indicate that it belongs to the very highly stable/highly stable regime (Barton et al. 2012). Figure 5 (c) on the other hand shows a deeper boundary layer with moderate stability suggesting that the group with medium cloud thickness (20 to 80%) is similar to the stable regime described by Barton et al. 2012. Note that the occurrence frequency of these two groups (Table 1) also aligns with that of the respective regimes observed during fall (Barton et al. 2012).

A comparison of the lower tropospheric stability and BL (cloud-top) height between both groups (Table 1 and Figs. 5 (c), (d)) reveal that they are in fact analogous to the stratocumulus and stratus cloud types. The stable, shallow, and cloudy

boundary layer in Fig. 5 (d) is characteristic of the stratus cloud regime, whereas the deeper well-mixed BL with higher cloud top (Fig. 5 (c)) represents the stratocumulus-topped boundary layer. Similar distinctions between stratus and stratocumulus Arctic clouds were noted in previous studies as well (Sato et al. 2012). Thus, the low, medium, and high BL cloud thickness groups identified in Table 1, are henceforth referred to as the uplift, stratocumulus, and stratus regimes, respectively. Figure 6 compares the lower tropospheric structure of temperature and moisture for stratus and stratocumulus regimes. Consistent with Sato et al. (2012), it is evident that CAA is mainly responsible for the occurrence of stratocumulus clouds (Fig. 6 (a)) whereas warm and moist air advection (or subsidence) leads to the formation of stratus clouds in the Arctic (Fig. 6).

Table 1 shows the average wind speed, ΔT, and the correlation coefficient (r) between SSHF and BL height, for the three regimes. The wind speeds are comparable, but the ΔT is significantly higher for the stratocumulus regime (99% confidence level). In the past, there has been speculation that the surface-generated turbulence is enhanced due to strong air-sea temperature gradients associated with cold air advection over open water (Sato et al. 2012; Kay and Gettelman 2009). Yet, the weak correlation coefficient (r) for the stratocumulus regime in Table 1 suggests that despite the enhanced ΔT, the surface sensible heat flux appears to contribute very little to the formation of the deep well-mixed boundary layer (Table 1). Figure 6 (a) shows that the temperature anomaly in this regime is maximized between 0.3 to 1.5 km altitudes, indicating that cold air advection occurs *above* the surface, where stratocumulus clouds likely form by the release of latent heat of vaporization. In such a case, the unstable lapse rate is perhaps more strongly driven by cloud condensational processes rather than the SSHF. This will be further explored in Section 4.4.

On the other hand, the surface contribution to boundary layer mixing is significant during the uplift regime, as well as in the presence of stratus clouds occurring within a (warm and wet) subsiding environment (r in Table 1). Other studies have also noted that the influence of surface type (sea ice vs. open water) is more evident for shallow boundary layer clouds occurring in the highly stable (stratus) regime compared to the stable (stratocumulus) regime (Barton et al. 2012; Taylor et al. 2015). In the following subsection, we will more closely examine the relationship between the SSHF and BL height in the uplift and stratus regimes.

4.2.2 Influence of surface winds

Figure 7 (a) shows that the SSHF can explain a substantial amount of the BL height variability in the uplift regime (up to 37%). For the stratus cloud regime, the correlation between SSHF and BL height is already significant (Table 1) but improves substantially during episodes of high (> 9.8 ms^{-1}) surface wind speed (Fig. 7 (b)). For the deep, stratocumulus-topped boundary layer, the relationship between SSHF and BL height becomes weakly positive ($r = 0.14$) during high surface wind speeds but remains insignificant. Thus, apart from other factors, surface winds are clearly important for generating turbulent heat exchange in the stable Arctic boundary layer.

Altogether, based on the linear relationships between SSHF and BL height and the frequency of occurrence of the uplift (~15%) and stratus cloud regimes (~41%), the surface-generated turbulence may explain up to 10% of the Arctic BL height variability during fall. Whereas the in-cloud moist and radiative processes that are responsible for formation of mixed layers over sea ice (Tjernstrom et al. 2004; Shupe et al. 2013; Morrison et al. 2012) are likely to be dominant over the open ocean as well. In the following subsection, we examine the interannual variability in the BL height and its relationship to the SSHF.

4.3 Interannual variability

As discussed in the previous section (4.2.3), the height of the well-mixed Arctic BL is likely controlled by the cloud-generated turbulence rather than the SSHF. Figure 8 shows the yearly distribution of BL height, BL cloud thickness ratio, and surface pressure, for the period of the cruise. Unlike the SSHF (Fig. 3 (a)), the BL height shows increases in its maximum values during recent years (2010, 2013). It also has greater interannual variability as suggested by the significantly shallow boundary layer (95% confidence level) observed during 2002 (Fig. 8 (a)). The large-scale circulation (sea level pressure distribution) appears to be different during this year (Fig. 8 (c)). The circulation anomaly may have a significant influence on the BL cloud distribution (Fig. 8 (b)), which may consequently impact the BL height variability (Fig. 8 (a)). (This will be elaborated in the following subsection).

The interannual variability in the correlation coefficient (r; Table 2) suggests that the SSHF and BL height relationship is most significant for the years 2002 and 2010 (99% confidence level). The time-series of both quantities indeed confirms the dominant role of surface fluxes in the evolution of the Arctic BL (Fig. 9). The reasons for the same are explored below.

As described in section 4.2, both cloud-type and wind speeds may influence the SSHF contribution to BL mixing. The frequency distribution of different cloud regimes and the corresponding surface wind speed anomalies (positive only) are shown for each year in Fig. 10. For the years with positive Arctic Oscillation (Table 2), it is evident that the stratus and stratocumulus regimes dominate the climate. The regime distribution is quite different during 2002 and 2013 (both years with negative AO index). The year 2002 is governed by anomalously low surface pressure or the uplift regime, whereas the year 2013 is accompanied by greater than usual occurrence of stratocumulus clouds (bottom panel of Fig. 10). Sampling inconsistency due to spatially restricted (fixed point) observations can also contribute to the anomalous cloud regime distribution observed during 2013. From Fig.10, it appears that a lower stratocumulus cloud fraction (bottom panel) coupled with higher surface wind speeds in the stratus regime (top panel), contribute to the better correlation between SSHF and BL height during 2002 and 2010 (Table 2).

Thus, although the SSHF presently controls only 10% of the BL height variability, the relationship can become stronger under more frequent occurrences of the uplift regime and/or high surface wind speeds associated with the stratus regime. As a result, the changing patterns of future Arctic climate, such as more frequent storms and greater wind stress (Hakkinen et al. 2008; Higgins and Cassano 2009; Smedsrud et al. 2011), may act to enhance the ocean-atmosphere

8

coupling. In the following section, we will further evaluate the relative roles of SSHF and clouds in atmospheric mixing based on boundary layer thermodynamics.

4.4 Boundary layer thermodynamics over the open Arctic Ocean

The contribution of SSHF to BL mixing is better understood by examining its role in the thermodynamic equation (Eq. 2).

$$\int_0^{BL} \frac{\partial T}{\partial t} + \int_0^{BL} \bar{V}\nabla T + \int_0^{BL} (\Gamma_{adiabat} - \Gamma_{env})w = \int_0^{BL} \frac{Q}{c_p}$$

(A)   (B)   (C)   (D)

where A = time-rate of change in local temperature

      B = horizontal temperature advection in the BL

      C = product of the vertical velocity and the difference between the adiabatic and environment lapse-rates.

      D = diabatic heating/cooling caused by surface turbulent fluxes, cloud (condensational/evaporative) processes, and

          radiative mechanisms.

The explanation of various terms in Eq. (2) can be found in Holton (2004). The measure of the atmospheric stability (Term C) is zero, by definition, for a well-mixed boundary layer because the environmental lapse-rate (Γ_{env}) equals the dry/moist adiabatic lapse-rate ($\Gamma_{adiabat}$; see Section 3.2). We inspect processes (sources of vertical motions) that are necessary to make Γ_{env} equal to the $\Gamma_{adiabat}$ If we assume that horizontal thermal advection (term B) is homogenous leading to uniform changes in the local temperature profile (term A), then it may not influence the atmospheric stability (Γ_{env}). However, Γ_{env} can change in response to diabatic heating (term D), which includes two main sources viz., surface (sensible and latent) heat fluxes and clouds.

The largely positive temperature gradient (ΔT) during early fall (Fig. 3 (b)) is favourable for episodes of upward sensible heat flux and rising air parcels which can make Γ_{env} more unstable. (Note that although the surface latent heat fluxes are not measured here, they are typically proportional to the SSHF). Similarly, Arctic clouds which form due to large-scale processes (Herman and Goody 1976; Morrison et al., 2012; Solomon et al., 2014), can generate vertical mixing due to a combination of condensational warming and cloud-top radiative cooling. Now, in the absence of low-clouds, the surface fluxes will be the main factor to control Γ_{env} and the BL mixing. This is consistent with our results, which basically show a good correlation between the SSHF and BL height for the cases with near-zero BL cloud thickness (uplift regime in Table 1 and Fig. 7 (a)). On the other hand, when low-clouds are observed in the vicinity of well-mixed layers (stratus and stratocumulus regimes in Table 1), a weaker relationship is found to exist between the SSHF and BL height as cloud

9

condensational warming may enhance the height of the surface mixed layer. The shallow BL observed in 2002 is likely due to the lack of occurrence of low-clouds during that year (Fig. 8 (a), (b)).

Now, let us consider the large-scale environment associated with cloudy Arctic BLs. It appears that CAA leads to stratocumulus cloud formation whereas stratus clouds occur in a warm and wet environment (Figs. 5 and 6; Sato et al. 2012). One might expect the SSHF contribution to be greater (cloud contribution to be lower) during the former regime due to the larger ΔT associated with CAA (Table 1). But, we find no significant relationship between the BL height and ΔT as explained in section 4.2. The BL mixing due to SSHF is only favoured during strong winds in the stratus regime (Fig. 7 (b)). For the stratocumulus regime, it is possible that the advected cold air sinks to dampen the SSHF-generated mixing, but also simultaneously lowers the dew point temperature to favour cloud formation and cloud-generated turbulence. Contrary to our findings, a recent modelling study by Deser et al. (2010) showed that during October to April over an ice-free Arctic Ocean, CAA is nullified by the substantial release of surface heat fluxes with minimal contribution from cloud condensational warming. It is therefore imperative to re-evaluate the role of diabatic heating sources in Arctic climate models, especially check the heightened sensitivity to air-sea temperature gradients. Clearly, cloud-driven turbulence and condensational warming can play a significant role in the Arctic boundary layer. In the future, the attribution of moisture involved in BL cloud condensation processes, including the relative importance of remote vs. local sources, remains to be explored.

5 Discussions

5.1 Non-local relationship between sea ice, BL, and clouds

While it is clear that the early fall open Arctic Ocean has a deeper well-mixed boundary layer and a higher cloud-base compared to its ice-covered counterpart (Sato et al. 2012; Schweiger et al. 2008; Kay and Gettelman 2009), the role of surface fluxes remains to be explored. The deepest, most convective BL (stratocumulus cloud regime) appears to develop in association with large-scale advection of cold, dry air, with minimum contribution from surface sensible heat flux (Figs. 5 (c) and 6). But it is possible that latent heating via increased surface moisture fluxes (Boisvert and Stroeve 2015; Boisvert et al. 2015) contributes to the observed boundary layer and cloud changes. For example, Boisvert and Stroeve (2015) estimated a positive correlation between surface moisture flux and cloud fraction in the Beaufort and Chukchi sea regions during the month of October. However, they did not observe such a relationship in September. In the past, studies have commonly observed that northerly cold-air outbreaks originating from polar ice caps result in roll convection and cloud streets fuelled primarily by the substantial input of moisture from the ice-free ocean to the atmosphere (Brümmer 1999; Brümmer and Pohlmann 2000; Hartmann et al. 1999). Therefore, in addition to local increases in the surface heat and moisture fluxes, the retreating boundaries of the summer Arctic sea ice are important for frontal dynamics that occur along marginal sea ice zones (Kolstad and Bracegirdle 2008).

Some model simulations of an ice-free Arctic Ocean suggest that the surface heat fluxes will dominate polar amplification during fall and early winter (Deser et al. 2010; Tietsche et al. 2011; Higgins and Cassano 2009). Our results

10

suggest that surface fluxes *and* clouds produce diabatic heating in the Arctic BL, and are both highly sensitive to non-local dynamical factors. This interaction between dynamic and thermodynamic variables must be duly incorporated in climate models for accurate projections of polar amplification. Moreover, the radiative feedbacks of various cloud types to the darker, ice-free ocean surface also need to be well-represented in climate models.

5.2 Implications for sea ice recovery mechanisms

During late summer and early fall, the turbulent heat loss from the ocean is considered important for initiating refreeze processes (Inoue and Hori 2011; Tietsche et al. 2011). Our study shows that the efficiency of turbulent heat exchange has not increased substantially over the regions that have recently experienced accelerated summer sea ice loss. Thus, we strongly recommend continuing the exploration of mechanisms that contribute to the cooling of the ocean and the recovery of the fast declining Arctic sea ice.

Model simulations may have a more optimistic representation of the ocean-atmosphere interactions in the dynamic new ice-free Arctic, which appears to be sensitive to the temperature gradient (ΔT) at the surface (Deser et al. 2010; Tietsche et al. 2011; Schweiger et al. 2008; Higgins and Cassano 2009). For example, simulations show that the complete loss of summer ice over the Arctic Ocean will be reversed during the following cold season, viz. October-December, when ΔT is positive (Tietsche et al. 2011). However, more recent measurements have shown that the ocean heat gained during summer can be sustained over the period of fall and winter without being immediately dissipated to the atmosphere, thereby slowing the recovery of sea ice (Jackson et al. 2010; 2012). Based on our results, it appears that conditions of uplift and high surface wind speeds may favour efficient heat dissipation by SSHF, whereas episodes of CAA may favour latent heat fluxes. Nilsson et al. (2001) similarly found that the late summer/early fall turbulent heat fluxes over the Atlantic sector of the open Arctic Ocean can be sensitive to cyclone activity and cloud regimes. These dynamical triggers should be duly considered in BL parameterization schemes and surface layer schemes of climate models while evaluating future scenarios and sea ice recovery mechanisms for the Arctic. The chances of possible irreversible and more permanent feedbacks of sea ice loss also need to be seriously evaluated in models.

6 Summary

For the rapidly evolving Arctic region, a comprehensive understanding of ocean-atmosphere interactions and underlying coupling processes is crucial for improving regional and global climate models and their predictability. Current models have significant differences in important physical processes such as the efficiency of turbulent heat transfer from the ocean to the atmosphere (Kolstad and Bracegirdle 2008; Grønas and Skeie 1999; Pagowski and Moore 2001). The primary goal of this study was to evaluate and quantify the role of open ocean sensible heat flux in Arctic BL turbulence based on multi-year ship-based observations acquired during early fall. The main conclusions are summarized as follows:

11

- The surface sensible heat flux during fall is mostly positive owing to the positive ocean-atmosphere temperature differences (ΔT) over the ice-free ocean. Yet, the instantaneous atmospheric response to enhanced heat fluxes only occurs during specific large-scale (cloud) regimes. It is favored during the uplift (low-pressure) regime (~ 15% of the cases) followed by the stratus cloud (warm subsidence) regime (~ 41% of the cases). Additionally, the ocean heat dissipation by SSHF is more efficient during episodes of high surface wind speeds compared to increased ΔT.

- Stratus and stratocumulus clouds are frequently observed in the open Arctic boundary layer, prevalent roughly 85% of the time (Fig. 10). The year 2002 is an exception with low BL cloud thicknesses due to the anomalously low surface pressure conditions. In agreement with previous work (Sato et al. 2012), it is found that stratus clouds are associated with warm air advection and a shallow BL (high stability), whereas stratocumulus clouds result from CAA and have deeper, well-mixed BLs (low stability). Contrary to speculation, the turbulence generated by surface heat fluxes is more strongly favored in the former compared to the latter. Whereas the instability associated with the stratocumulus-topped BL is likely caused by cloud-driven (moist adiabatic and radiative) turbulent processes, and is perhaps enhanced by upward surface moisture fluxes over the open ocean.

- Consistent with previous studies (Sato et al. 2013, Schweiger et al. 2008), it is evident that the BL height has increased over the ice-free Arctic Ocean in recent years (Fig. 8 (a)). However, as suggested by past observations over late-summer sea ice (Tjernstrom et al. 2004; Shupe et al. 2013; Morrison et al. 2012), its variability is primarily controlled by the atmospheric circulation and low-cloud regime as opposed to surface heat fluxes. The relationship between SSHF and BL height is characterized by strong interannual variability, influenced by both surface wind speeds and cloud regimes. In general, the dynamical forcing appears to dominate the ocean-atmosphere coupling during early fall.

This study highlights the need for comprehensive in-situ observations to improve model physics for more reliable projections of the coupled Arctic climate and sea ice in the future. Using available surface and upper-air observations from ship cruises, we provide first-hand insights of the optimal conditions for the SSHF contribution to atmospheric mixing. The relevant coupling mechanisms identified in this study, especially the influence of large-scale circulation patterns on clouds and SSHF, can be incorporated to improve the simulations of sea ice loss in current climate models, and to obtain a more realistic view of its long-term effects on Arctic climate. The role of latent heat fluxes and cloud formation were evaluated using proxy measurements, nevertheless, it appears to be rather important for the Arctic BL stability. The regional and seasonal scale variability in SSHF and BL height warrants further investigation as well, which will be pursued in future studies.

MR13-06 Leg 1 cruises of R/V Mirai, Japan Agency for Marine-Earth Science and Technology. The Arctic Oscillation Index values were obtained from the National Oceanic and Atmospheric Administration's Climate Prediction Center using the following webpage: http://www.cpc.ncep.noaa.gov/products/precip/CWlink/daily_ao_index/ao.shtml.

References

5   Barton, N. P., S. A. Klein, J. S. Boyle, and Y. Y. Zhang, 2012: Arctic synoptic regimes: Comparing domain-wide Arctic cloud observations with CAM4 and CAM5 during similar dynamics, *J. Geophys. Res*., 117, D15205, doi:10.1029/2012JD017589.

Boisvert, L. N., T. Markus, and T. Vihma, 2013: Moisture flux changes and trends for the entire Arctic in 2003–2011 derived from EOS Aqua data, *J. Geophys. Res. Oceans*, 118, 5829–5843, doi:10.1002/jgrc.20414.

10 Boisvert, L. N., and J. C. Stroeve, 2015: The Arctic is becoming warmer and wetter as revealed by the Atmospheric Infrared Sounder. *Geophys. Res. Lett*., 42, 4439–4446. doi:10.1002/2015GL063775.

Brümmer, B. ,1999: Roll and cell convection in wintertime arctic cold-air outbreaks, *J. Atmos. Sci*., 56, 2613 – 2636.

Brümmer, B., and S. Pohlmann, 2000: Wintertime roll and cell convection over Greenland and Barents Sea regions: A climatology, *J. Geophys. Res*., 105, 15,559 – 15,566.

15 Bourassa, M.A., S.T. Gille, D.L. Jackson, J.B. Roberts, and G.A. Wick., 2010: Ocean winds and turbulent air-sea fluxes inferred from remote sensing. *Oceanography,* 23(4), 36–51

Curry, J. A., and co-authors, 2000: FIRE Arctic clouds experiment. *Bulletin of the American Meteorological Society*, *81*(1), 5-29.

Deser, C., R. Tomas, M. Alexander, and D. Lawrence, 2010: The seasonal atmospheric response to projected Arctic sea ice

20 loss in the late twenty-first century. *Journal of Climate*, 23(2), 333-351.

Eastman, R., and S. G. Warren, 2010: Interannual Variations of Arctic Cloud Types in Relation to Sea Ice. *J. Climate*, 23, 4216–4232.

Fairall, C.W., E.F. Bradley, D.P. Rogers, J.B. Edson, and G.S. Young, 1996: Bulk parameterization of air–sea fluxes in TOGA COARE. *Journal of Geophysical Research* 101(3), 747–3767.

25 Fujiyoshi, Y., and K. Shimada, 2002: R/V Mirai Cruise Report MR02-K05 Leg 1, Japan Agency for Marine-Earth Science and Technology, Yokosuka, Japan.

Fujiyoshi, Y., and K. Shimada, K., 2004: R/V Mirai Cruise Report MR04-05, Japan Agency for Marine-Earth Science and Technology, Yokosuka, Japan.

Grønas, S., and P. Skeie, 1999: A case study of strong winds at an Arctic front. *Tellus A, 51*(5), 865–879.

30 Hakkinen, S., A. Proshutinsky, and I. Ashik, 2008: Sea ice drift in the Arctic since the 1950s. *Geophysical Research Letters*, 35(19).

13

Hartmann, J., et al., 1999: Arctic radiation and turbulence interaction study, *Polar Res. Rep.* 305, 81 pp., Alfred Wegener Inst. for Polar and Mar. Sci., Potsdam, Germany

Herman, G., and R. Goody, 1976: Formation and persistence of summertime Arctic stratus clouds, *J. Atmos. Sci.*, 33, 1537–1553.

5   Higgins, M. E., and J. J. Cassano, 2009: Impacts of reduced sea ice on winter Arctic atmospheric circulation, precipitation, and temperature. *Journal of Geophysical Research: Atmospheres*, 114(D16).

Holton, J. R., 2004: *An introduction to dynamic meteorology*. Elsevier Academic Press.

Inoue, J., 2010: R/V Mirai Cruise Report MR10-05, Japan Agency for Marine-Earth Science and Technology, Yokosuka, Japan.

10   _____, 2013: R/V Mirai Cruise Report MR13-06, Japan Agency for Marine-Earth Science and Technology, Yokosuka, Japan.

_____, & M. E., Hori, 2011: Arctic cyclogenesis at the marginal ice zone: A contributory mechanism for the temperature amplification? *Geophysical Research Letters*, *38*(12).

_____, _____, T. Enomoto, & T. Kikuchi, 2011: Intercomparison of surface heat transfer near the Arctic marginal ice

15   zone for multiple reanalyses: A case study of September 2009. *Sola*, *7*, 57-60.

_____, and K. Yoneyama, 2009: R/V Mirai Cruise Report MR09-03, Japan Agency for Marine-Earth Science and Technology, Yokosuka, Japan.

_____, B. Kosović, and J. A. Curry, 2005: Evolution of a storm-driven cloudy boundary layer in the Arctic. *Boundary-layer meteorology*, *117*(2), 213-230.

20   _____, and others, 2015: Additional Arctic observations improve weather and sea-ice forecasts for the Northern Sea Route., *Sci. Rep.*, 5, 16868.

Jackson, J. M., E. C. Carmack, F. A. McLaughlin, S. E. Allen, and R. G. Ingram, 2010: Identification, characterization, and change of the near-surface temperature maximum in the Canada Basin, 1993–2008. *Journal of Geophysical Research: Oceans*, 115(C5).

25   Jackson, J. M., W. J. Williams, and E. C. Carmack, 2012: Winter sea-ice melt in the Canada Basin, Arctic Ocean. *Geophysical Research Letters*, 39(3).

Kalnay, E., and others, 1996: The NCEP/NCAR 40-year reanalysis project. *Bulletin of the American meteorological Society*, *77*(3), 437-471.

Kawaguchi, Y., S. Nishino, and J. Inoue, 2015: Fixed-Point Observation of Mixed Layer Evolution in the Seasonally Ice-

30   Free Chukchi Sea: Turbulent Mixing due to Gale Winds and Internal Gravity Waves. *J. Phys. Oceanogr.*, **45**, 836–853.

Kay, J. E., & A. Gettelman, 2009: Cloud influence on and response to seasonal Arctic sea ice loss. *Journal of Geophysical Research: Atmospheres (1984–2012)*, *114*(D18).

14

Klein, S. A., and co-authors, 2009: Intercomparison of model simulations of mixed–phase clouds observed during the ARM Mixed–Phase Arctic Cloud Experiment. I: Single–layer cloud. *Quarterly Journal of the Royal Meteorological Society*, *135*(641), 979-1002.

Kolstad, E. W., & T. J. Bracegirdle, 2008: Marine cold-air outbreaks in the future: an assessment of IPCC AR4 model results for the Northern Hemisphere. *Climate Dynamics*, *30*(7-8), 871-885.

Kurita, N., and K. Yoneyama, 2008: R/V Mirai Cruise Report MR08-04, Japan Agency for Marine-Earth Science and Technology, Yokosuka, Japan.

Morrison, H., and co-authors, 2011: Intercomparison of cloud model simulations of Arctic mixed-phase boundary layer clouds observed during SHEBA/FIRE-ACE, *J. Adv. Model. Earth Syst.*, 3, M05001

Morrison, H., G. de Boer, G. Feingold, J. Harrington, M. D. Shupe, and K. Sulia, 2012: Resilience of persistent Arctic mixed-phase clouds. *Nature Geoscience*, *5*(1), 11-17.

Nicholls, S. and J. Leighton, 1986: An observational study of the structure of stratiform cloud sheets: Part I. Structure. *Q.J.R. Meteorol. Soc.,* 112, 431–460. doi: 10.1002/qj.49711247209

Nilsson, E. D., Ü. Rannik, & M. Håkansson, 2001: Surface energy budget over the central Arctic Ocean during late summer and early freeze–up. *Journal of Geophysical Research: Atmospheres (1984–2012)*, *106*(D23), 32187-32205.

Pagowski, M., and G. Moore, 2001: A numerical study of an extreme cold- air outbreak over the Labrador Sea: sea ice, air–sea interaction, and development of polar lows. *Mon. Weather Rev.,* 129, 47–72

Palm, S. P., S. T. Strey, J. Spinhirne, and T. Markus, 2010: Influence of Arctic sea ice extent on polar cloud fraction and vertical structure and implications for regional climate, *J. Geophys. Res.*, 115, D21209, doi:10.1029/2010JD013900.

Sato, K., J. Inoue, Y. M. Kodama, & J. E. Overland, 2012: Impact of Arctic sea–ice retreat on the recent change in cloud–base height during autumn. *Geophysical Research Letters*, *39*(10).

Schweiger, A. J., R. W. Lindsay, S. Vavrus, & J. A. Francis, 2008: Relationships between Arctic sea ice and clouds during autumn. *Journal of Climate*, *21*(18), 4799-4810.

Shupe, M. D., and co-authors, 2013: Cloud and boundary layer interactions over the Arctic sea-ice in late summer. *Atmospheric Chemistry and Physics Discussions*, *13*(5), 13191-13244.

Smedsrud, L. H., A. Sirevaag, K. Kloster, A. Sorteberg, and S. Sandven, 2011: Recent wind driven high sea ice area export in the Fram Strait contributes to Arctic sea ice decline. *The Cryosphere*, 5(4), 821-829.

Solomon, A., and others, 2014: The sensitivity of springtime Arctic mixed-phase stratocumulus clouds to surface-layer and cloud-top inversion-layer moisture sources, *J. Atmos. Sci.*, 71, 574–595.

Taylor, P. C., S. Kato, K.-M. Xu, and M. Cai, 2015: Covariance between Arctic sea ice and clouds within atmospheric state regimes at the satellite footprint level, *J. Geophys. Res. Atmos.*, 120, 12,656–12,678, doi:10.1002/ 2015JD023520.

Tietsche, S., D. Notz, J. H. Jungclaus, and J. Marotzke, 2011: Recovery mechanisms of Arctic summer sea ice. *Geophysical Research Letters*, *38*(2).

15

Tjernström, M., and co-authors, 2004: The summertime Arctic atmosphere: Meteorological measurements during the Arctic Ocean Experiment 2001. *Bulletin of the American Meteorological Society* 85.9.

Wu, D. L., and J. N. Lee, 2012: Arctic low cloud changes as observed by MISR and CALIOP: Implication for the enhanced autumnal warming and sea ice loss. *Journal of Geophysical Research: Atmospheres (1984–2012)*, *117*(D7).

5   **Tables**

Table 1. The frequency of occurrence, mean surface pressure, mean lower tropospheric stability, mean boundary layer height, cloud regime, the correlation coefficient (r) between SSHF and BL height, mean temperature difference between ocean and air, and mean surface wind speed, observed for the three different groups of BL cloud thickness ratio (see text and Fig. 5 for explanation). Statistically significant values of r (99% confidence level) are highlighted in bold.

BL cloud thickness ratio (%)	≤ 20	20 to 80	≥ 80
Occurrence frequency (%)	15	44	41
Surface Pressure (mb)	1008	1015	1014
θ_{700} - θ_{surf} (°C)	13.6	14.9	18.1
BL height (m)	646	997	508
Cloud Regime	Uplift	Stratocumulus (stable)	Stratus (very highly/highly stable)
r	**0.58**	-0.04	**0.33**
ΔT (°C)	1.76	3.41	1.71
V_{surf} (m.s^{-1})	7.01	7.20	7.05

10

Table 2. The average Arctic Oscillation (AO) index observed during the period of the cruise, the correlation coefficient between SSHF and BL height (r), and the number of observations (n), for each cruise year. Statistically significant values of r (99% confidence level) are highlighted in bold.

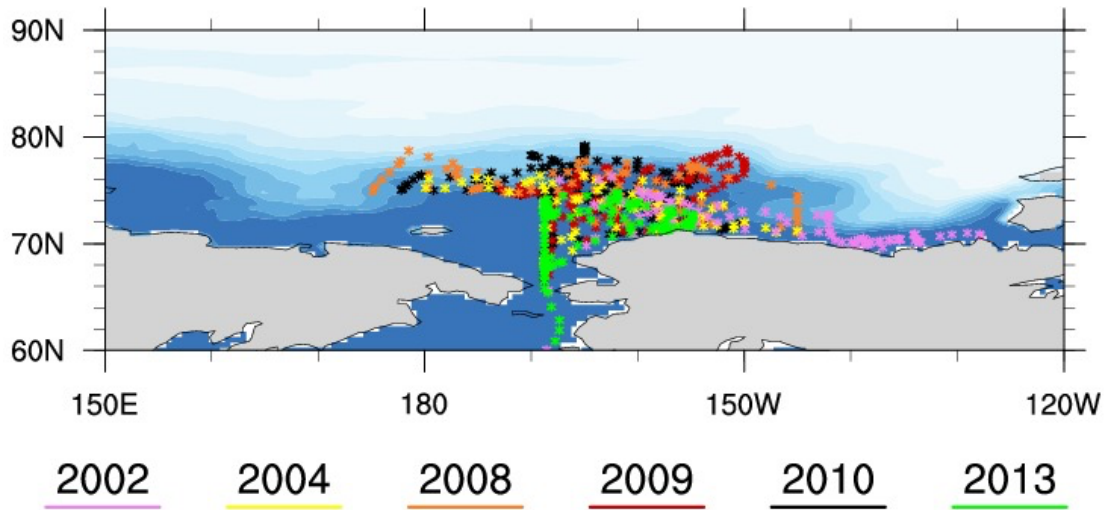| Year	2002	2004	2008	2009	2010	2013
AO Index	-1.16	0.08	1.21	0.29	0.51	-1.50
r	**0.64**	0.15	0.18	0.16	**0.59**	-0.02
n	100	65	93	131	214	273

15

16

Figures

Figure 1: Ship tracks during multi-year cruises of the R/V Mirai indicated by colored asterisk symbols. The average ice fraction (shaded white) at the time of cruise during 2008-2010 is also shown based on National Centers for Environmental Prediction/National Center for Atmospheric Research (NCEP/NCAR) reanalyses project (Kalnay et al. 1996).

17
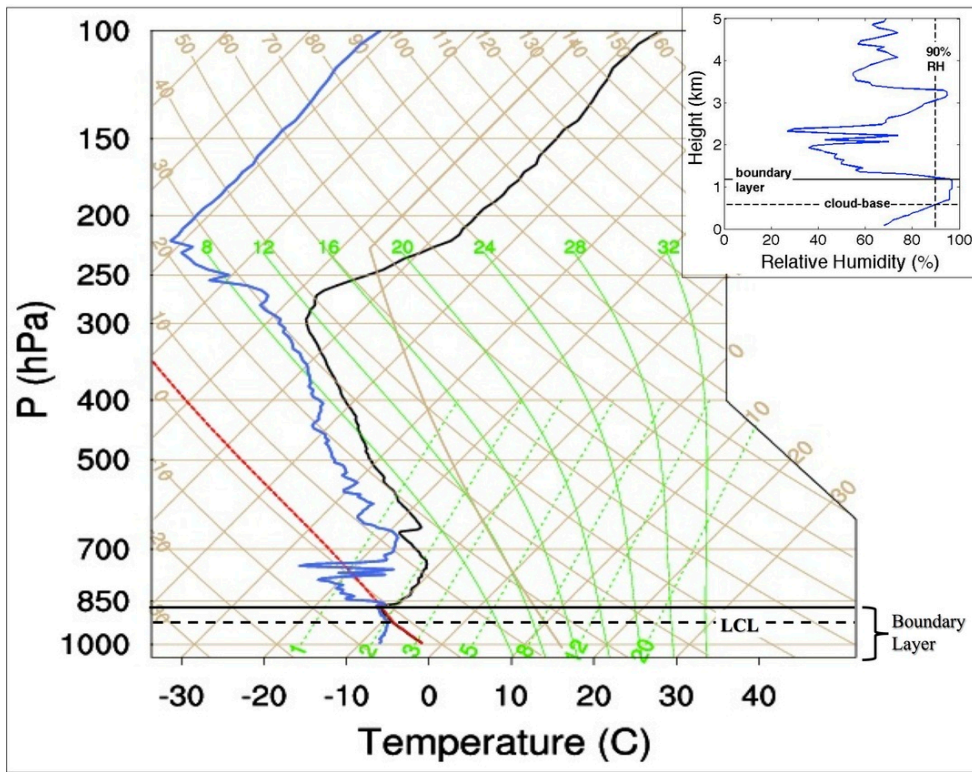
Figure 2: Skew T- log P diagram denoting the profiles of environmental temperature (black) and dew point temperature (blue) observed at 09Z September 21, 2013. The red dashed line represents the adiabatic ascent of a surface-based parcel. The solid horizontal black line is the boundary layer (BL) height determined using the parcel-based method, whereas the dashed horizontal black line represents the lifting condensation level or LCL; and (inset) a close examination of the relative humidity in the lowest 5 km, where the dashed vertical line represents the 90% RH threshold, the dashed horizontal line is the cloud-base, and the solid horizontal line represents the boundary layer. (For detailed description on the components of a skew T-log P chart, refer to the Air Weather Service technical report titled AWS/TR-79/006, *The Use of the Skew T, Log P Diagram in Analysis and Forecasting*, Dec.1979, revised March 1990).

18
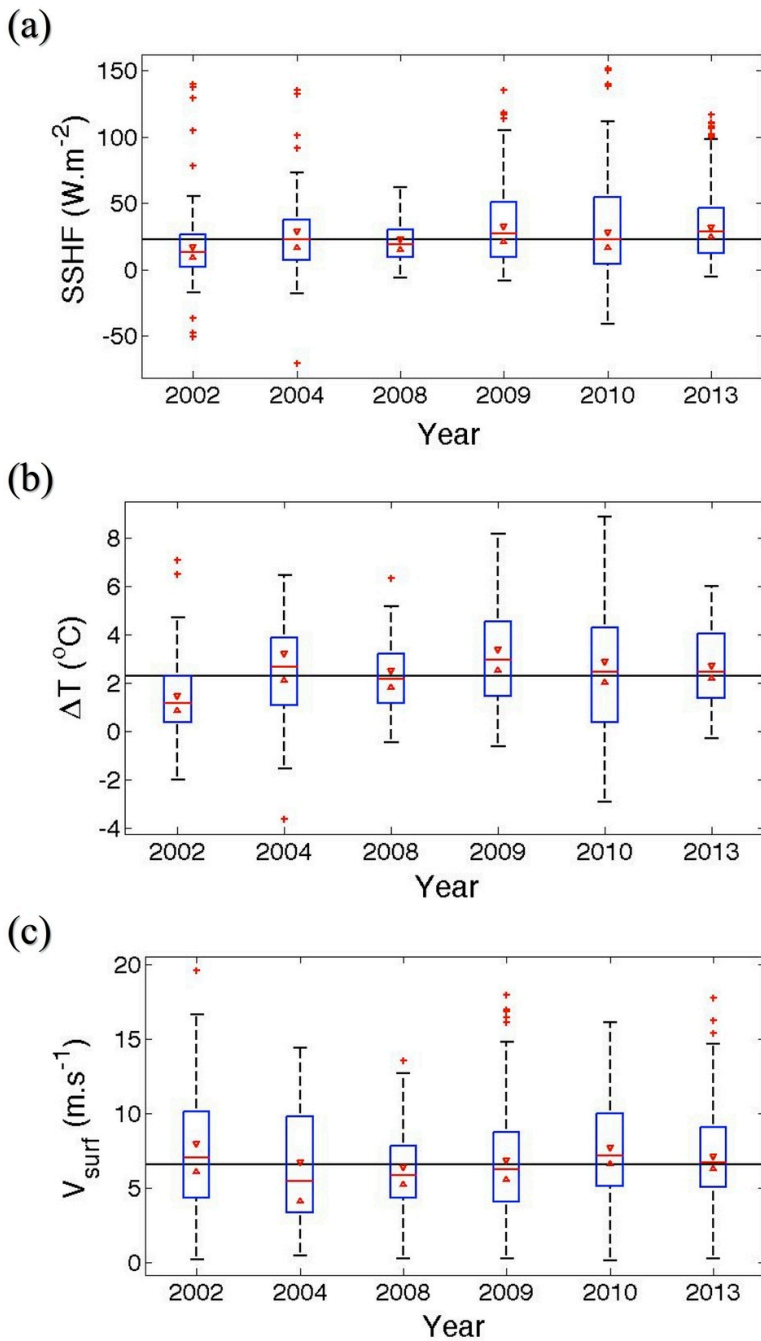
Figure 3: The interannual variability in the distribution of (a) the surface sensible heat flux (SSHF), (b) ocean-atmosphere temperature gradient (ΔT), and (c) surface wind speeds (V_{surf}). The solid horizontal black line represents the overall median value based on 6 years of ship data. The median for each year is represented by the horizontal red line within each boxplot, and the red notches represent the 95% confidence intervals around the same. Two medians are different at the 5% significance level if their intervals do not overlap.

19
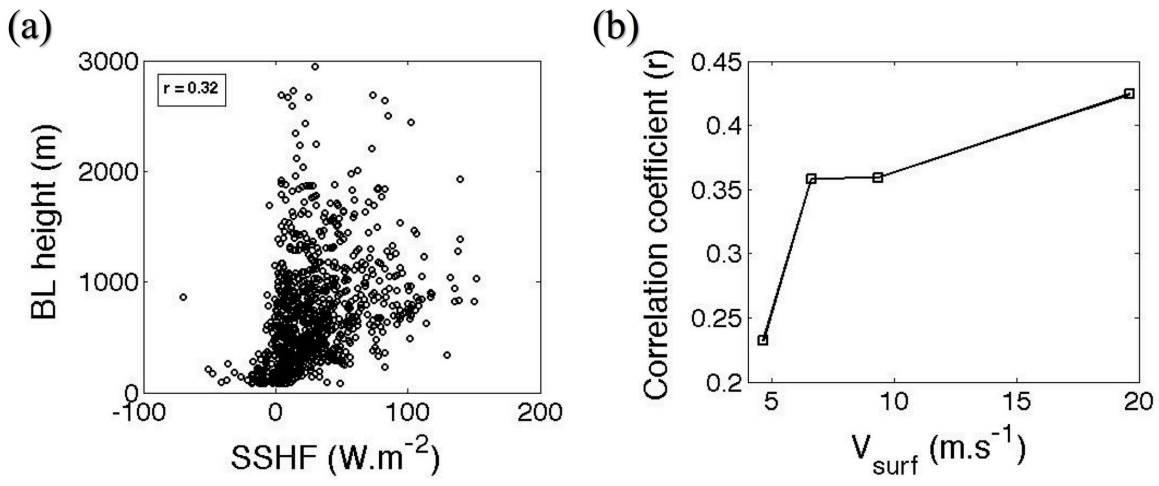
Figure 4: (a) Scatter plot of the SSHF and BL height using all observations based on 6 years of cruise-ship data. The correlation coefficient is denoted by *r*, and **(b)** *r* as a function of surface wind speed (V_{surf}). The data are binned based on the quartiles of V_{surf}, and *r* is calculated for each bin. The number of observations in each bin is equal to 219.
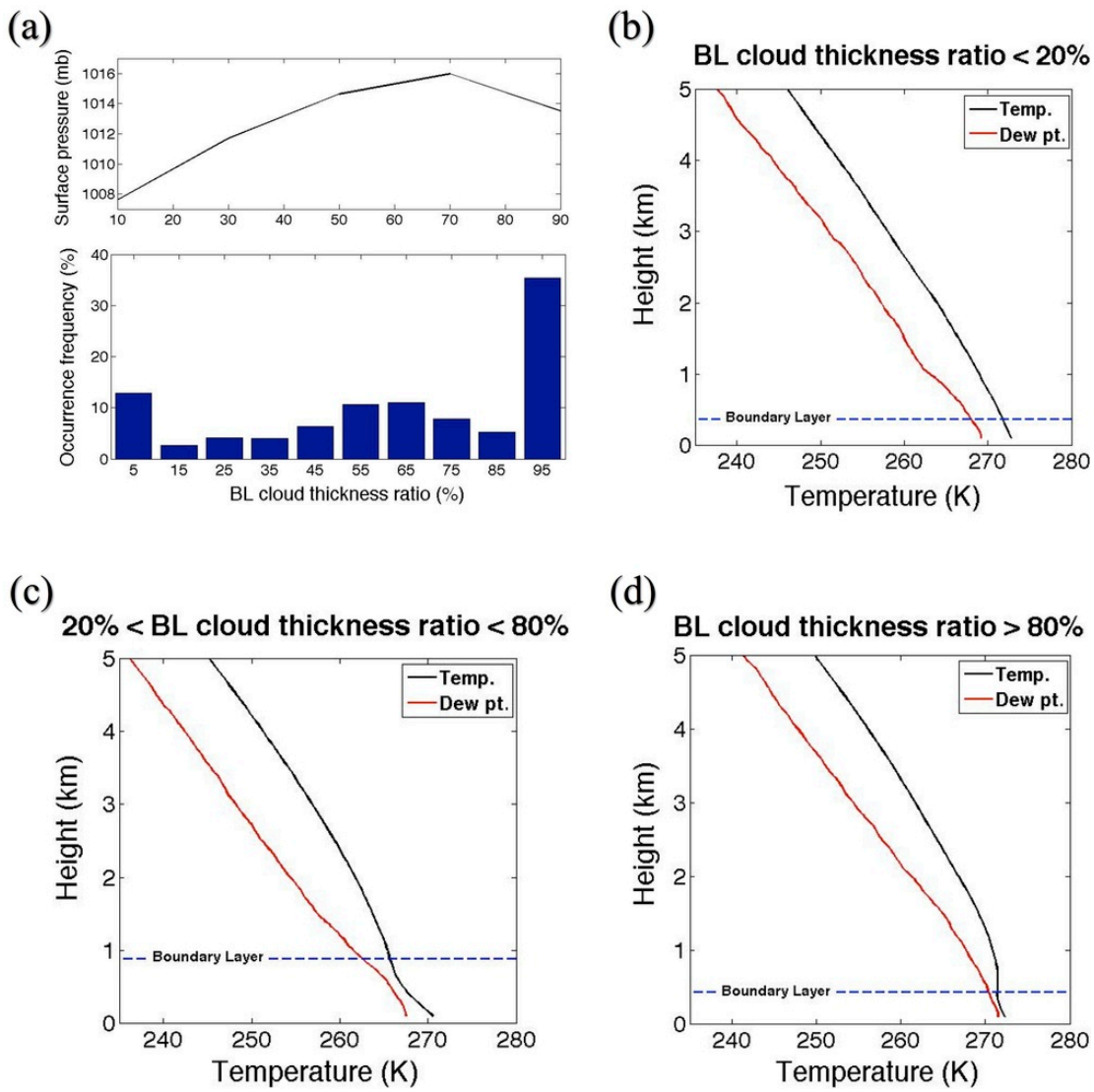
Figure 5: (a) The frequency distribution of BL cloud thickness ratio (bottom panel), and the mean surface pressure for 5 equally-spaced bins of the BL cloud thickness ratio (top panel), and (b) the profiles of mean temperature and dew point temperature observed for cases with BL cloud thickness ratio ≤ 20%, (c) same as (b) but for cases with 20% < BL cloud thickness ratio < 80%, and (d) same as (b) but for cases with BL cloud thickness ratio ≥ 80%.
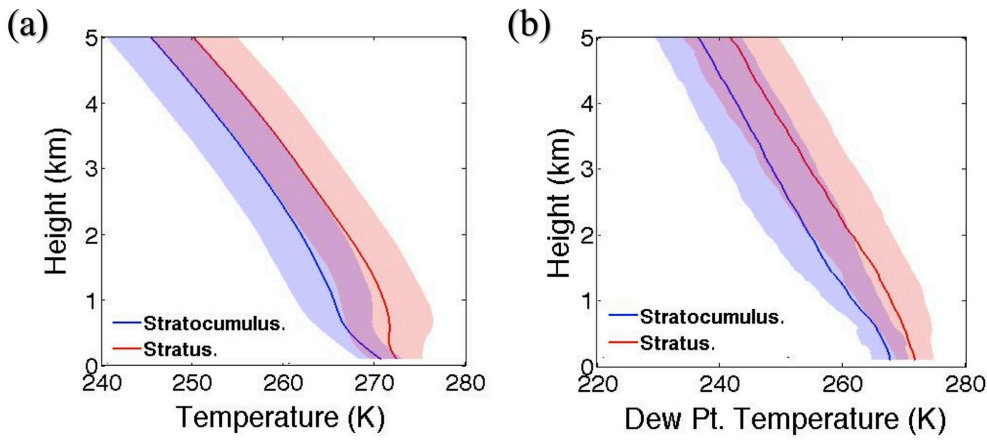
Figure 6: The atmospheric profile comparison between the stratocumulus and stratus regimes. The solid line represents the mean and the shaded area represents the standard deviation of (a) the temperature and (b) the dew point temperature.
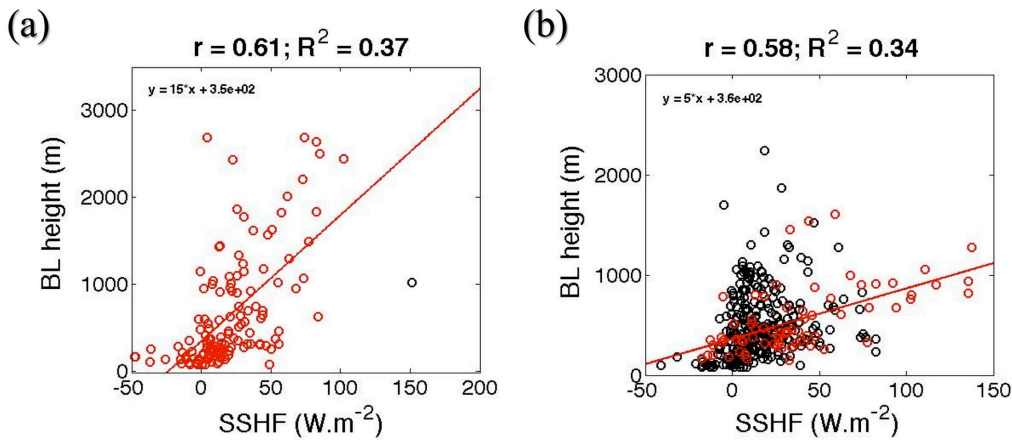
5

Figure 7: The scatter plot of SSHF and BL height during (a) the uplift regime, and (b) the stratus regime. The linear relationship between the SSHF and BL height derived using the least squares method of curve-fitting for (a) all cases (except one outlier indicated by black marker), and (b) cases with surface wind speeds exceeding 9.8 ms^{-1} (indicated by red markers). The correlation coefficient and the coefficient of multiple determination for each linear relationship is denoted by *r* and R^2, respectively. Note that the outlier in the uplift regime is an observation point with maximum ΔT, which has no influence on *r*. Conversely, the red markers in the stratus regime are observations with maximum surface wind speeds, which have a positive influence on *r*. See section 4.2 for explanation.
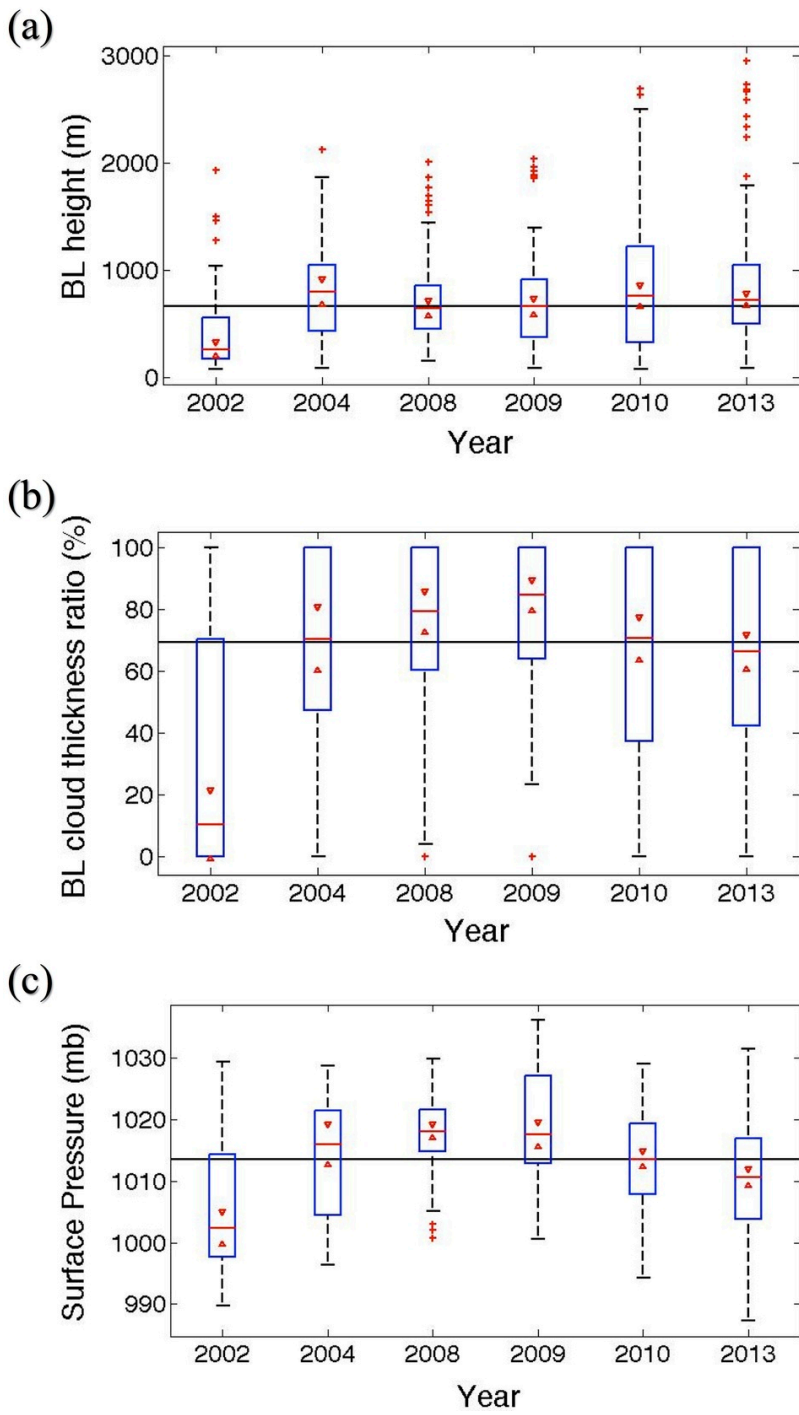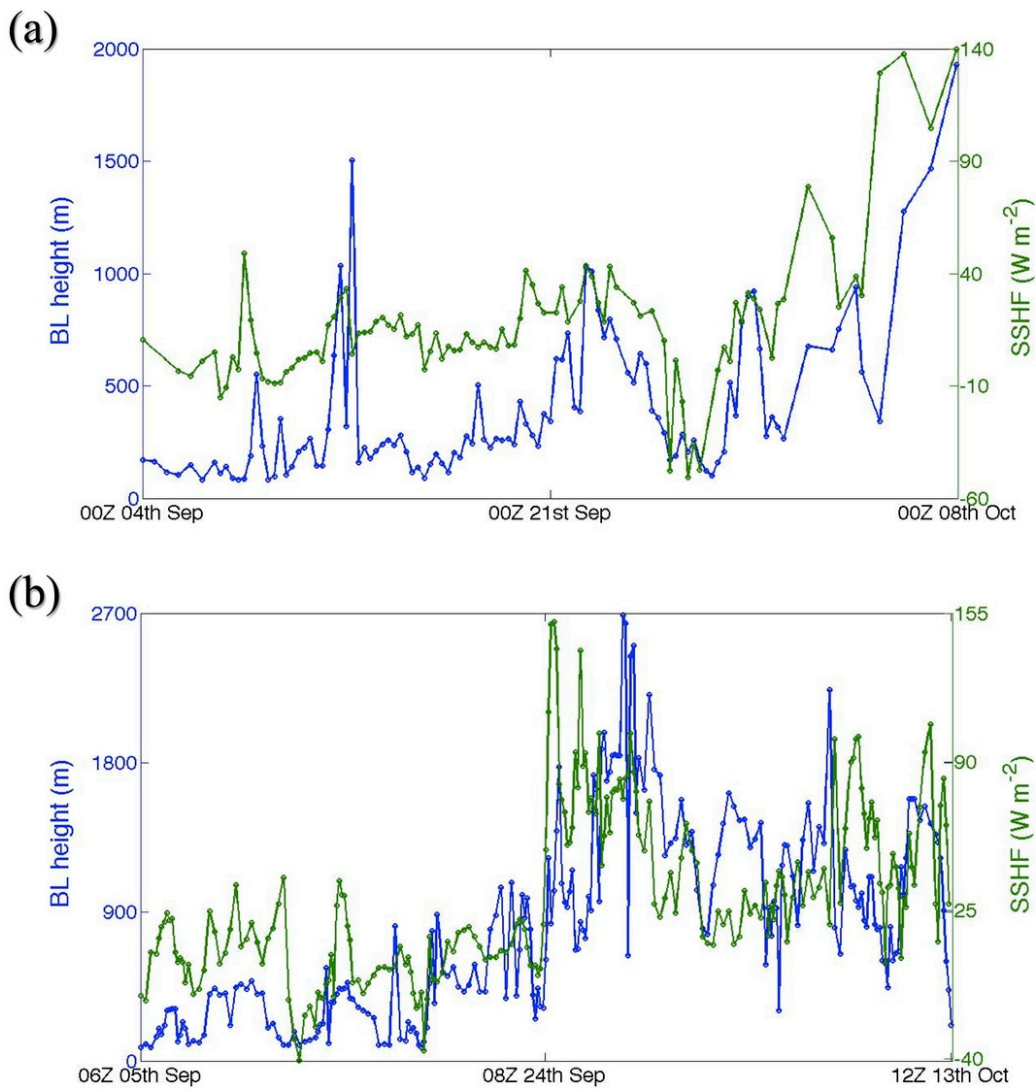
10

Figure 8: Same as Fig. 3 but for (a) boundary layer height, (b) boundary layer cloud thickness ratio, and (c) surface pressure.

23

Figure 9: The time-series of the boundary layer height (blue line; left axis) and the surface sensible heat flux (green line; right axis) during the period of the cruise in (a) 2002 and (b) 2010. The dots represent the time instances of actual measurements.
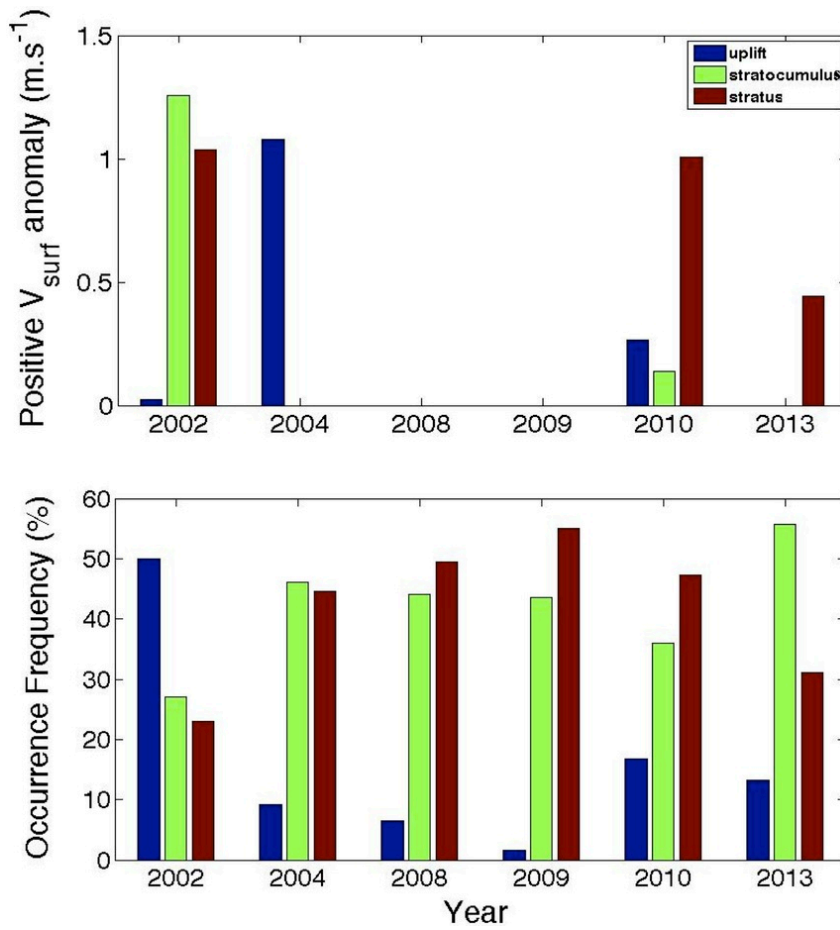
Figure 10: The distribution of occurrence frequency of the different cloud regimes within a given year (bottom panel), and the wind speed anomaly (positive only) for each year and each regime (top panel). Positive wind speed anomalies are calculated with respect to the mean wind speeds for the uplift, stratocumulus, and stratus regimes, which are 7, 7.2, and 7 ms^{-1}, respectively.

5